Agricultural and Forest Meteorology 355 (2024) 110104

Contents lists available at ScienceDirect

Agricultural and Forest Meteorology

journal homepage: www.elsevier.com/locate/agrformet

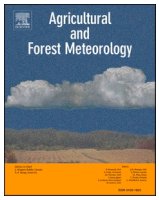

Aerosol interference with open-path eddy covariance measurement in a lake environment

Lei Jia [a], Mi Zhang [a,b,*], Wei Xiao [a,b], Yini Pu [c], Zhen Zhang [d], Hengxin Bao [a], Pei Ge [a], Jie Shi [a], Yang He [a], Fuyu Yang [a], Kelly Aho [e], Peter Raymond [f], Xuhui Lee [f,*]

[a] Yale-NUIST Center on Atmospheric Environment, Nanjing University of Information Science and Technology, Nanjing, Jiangsu Province, PR China
[b] Key Laboratory of Ecosystem Carbon Source and Sink, China Meteorological Administration (ECSS-CMA), Nanjing University of Information Science and Technology, Nanjing, Jiangsu Province, PR China
[c] Office of Development Planning and Discipline Construction, Chengdu University of Technology, Chengdu, Sichuan Province, PR China
[d] Nanjing Jiangning District Meteorological Bureau, Nanjing, Jiangsu Province, PR China
[e] Department of Earth & Environmental Sciences, Michigan State University, East Lansing, Michigan, USA
[f] School of the Environment, Yale University, New Haven, Connecticut, USA

ARTICLE INFO

Keywords:
Eddy covariance
Carbon dioxide flux
Lake
Aerosol

ABSTRACT

Open-path eddy covariance (OPEC) is widely used for measuring trace gas fluxes between the surface and the atmosphere. At a lake in Eastern China (Lake Taihu), the CO_2 flux measured with OPEC was often negative at night (with values as low as -22.1 μmol m^{-2} s^{-1}) and was coherent across the whole lake, as if the lake were a large sink of atmospheric CO_2. The purpose of this study is to investigate the cause of this negative flux phenomenon. In addition to OPEC, we also used closed-path eddy covariance (CPEC) and the transfer coefficient (TC) method to measure the flux. The results show that the persistent negative CO_2 flux phenomenon was observed with OPEC but not with CPEC or TC. Because air drawn into the CPEC analyzer was filtered but the OPEC analyzer was influenced by aerosol contamination, the most logical explanation was that particles deposited on the optical lens of the OPEC analyzer changed its cross-sensitivity to water vapor. The direct evidence of this interference was a strong positive correlation between the OPEC analyzer's signal strength and the CO_2 mixing ratio observed at 10 Hz. We suggest that it is possible to perform post-field correction to this negative flux bias using the 10 Hz signal strength data. In comparison, an OPEC system at a nearby land site did not experience aerosol interference due to low water vapor flux at night and lack of hygroscopic growth of particles on the optical lens in low humidity conditions. The type of aerosol interference reported here may also occur in high humidity and high pollution conditions elsewhere.

1. Introduction

Open-path eddy covariance (OPEC) is a technique widely used for measuring the exchanges of water vapor, carbon dioxide and other trace gasses between the surface and the atmosphere. Generally, an OPEC system consists of a sonic anemometer/thermometer for high frequency measurements of the 3-d wind vector and air temperature and a gas analyzer for measuring the concentrations of water vapor and carbon dioxide. Being exposed directly to ambient air, the analyzer is subject to a number of interreferences that must be corrected in order to obtain the true surface-air fluxes. The most well-known interference is the density effect caused by air density fluctuations arising from fluctuations in environmental temperature and water vapor concentration. This effect generally causes $\overline{w'\rho_c'}$, the covariance between the vertical velocity w and the CO_2 mass density ρ_c, to become more negative than the true flux. In environments where the underlying surface is not biologically active, such a dry and baren soil (Leuning et al., 1982) and a paved parking lot (Ham et al., 2003), the CO_2 flux without density correction will appear to be strongly negative at midday (e. g., -14 μmol m^{-2} s^{-1}) as if the surface were removing CO_2 from air at a fast rate. Here, we follow the standard micrometeorological sign convention: a negative flux is a flux directed towards the surface and a positive flux is a flux directed away from the surface. The WPL correction method effectively removes this density interference (Webb et al., 1980).

* Corresponding authors.
E-mail addresses: zhangm.80@nuist.edu.cn (M. Zhang), xuhui.lee@yale.edu (X. Lee).

https://doi.org/10.1016/j.agrformet.2024.110104
Received 25 January 2024; Received in revised form 30 May 2024; Accepted 3 June 2024

Several other types of interference have come to light since the publication of the WPL paper. Instrument self-heating, produced by the electronics in the sensor, by sensor absorption of solar radiation, or by application of a heater to prevent condensation on the optical window, can cause a negative CO_2 flux in land ecosystems in the cold season when photosynthetic CO_2 update is not expected (Amiro et al., 2010; Wang et al., 2016, 2017; Frank and Massman, 2020). The published studies show that this interference is mostly a daytime problem, suggesting that solar radiation may be the main source of sensor heating (Wang et al., 2016; Deventer et al., 2021). The resulting artificial CO_2 flux is on the order of -0.4 μmol m^{-2} s^{-1} (Deventer et al., 2021). In addition to density effects, laser-based gas analyzers are subject to a spectroscopic effect (Burba et al., 2019). When the CO_2 density is measured using a laser-based device, changes in temperature, H_2O and pressure affect the spectroscopic properties of the absorption line. The strength of this effect depends on the absorption line selected for detection. It is possible to select an absorption line whose spectroscopic effect mostly cancels out the density effect due to temperature variations (Pan et al., 2022). Another spectroscopic effect, known as cross-sensitivity to water vapor, arises from non-zero water vapor absorption of the light transmitted at the CO_2 absorption wavelength and from broadening of the CO_2 absorption line by water vapor pressure. This effect is generally corrected by manufacturer-determined coefficients (Kondo et al., 2014). In the marine environment, the cross-sensitivity to water vapor can result in CO_2 flux errors (Prytherch et al., 2010). Duan et al. (2013) show that this cross sensitivity causes an artificial negative flux on the order of -5.2 μmol m^{-2} s^{-1} in the North Yellow Sea. Some studies suggest that sea salt particles have led to greater cross sensitivity interference (Prytherch et al., 2010; Landwehr et al., 2014; Nilsson et al., 2018), although another study did not find evidence of this interference (Blomquist et al., 2014).

In this study, we report a type of interference with OPEC previously unknown in terrestrial environments. Our study site is Lake Taihu where large negative CO_2 flux was frequently observed. The negative flux almost always occurred at night and was spatially coherent across the lake. The nocturnal CO_2 flux can be as negative as -22.1 μmol m^{-2} s^{-1}. Lake Taihu is a large (area 2400 km^2) freshwater lake located in the highly urbanized Yangtze River Delta (YRD), Eastern China. Aerosol pollution is common occurrence. According to data released by the Bureau of Ecology and Environment of Suzhou, the annual mean PM2.5 concentration in Suzhou, a city located on the east coast of the lake, was 28 μg m^{-3} in 2022. The specific goals of our study are: (1) to compare the CO_2 flux measured with OPEC systems with that measured with a closed-path eddy covariance (CPEC) system and that measured with the transfer coefficient method (TC); (2) to compare the CO_2 flux measured at the lake with simultaneous OPEC and CPEC measurements at a land site also located in the YRD; (3) to examine the CO_2 signal strength of the gas analyzers at frequencies of eddy motion; and (4) to propose a method for correcting the OPEC CO_2 flux. Results are based on continuous observations that span a period of more than 12 years (from summer of 2010 to 2022) and with two types of broad-band open-path H_2O/CO_2 dual-gas analyzers. Multiple lines of evidence show that the negative CO_2 flux was not a biological signal but rather an artifact caused by aerosol interference with the OPEC analyzers. A potential underlying mechanism is alternation of the analyzer's cross-sensitivity to water vapor by hygroscopic growth of pollution particles deposited on its optical lens. Such aerosol interfere may also exist in other high-humidity and polluted environments.

2. Materials and methods

2.1. Site and instrumentation

Lake Taihu is a large subtropical lake in the eastern part of the YRD, located between 30° 5′ 40″ and 31° 32′ 58″N and 119° 52′ 32″ and 120° 36′ 10″ E (Fig. 1). The lake area is about 2400 km^2 and the average depth is 1.9 m. The measurement program is called the Taihu Eddy Flux Network. Details of the site and instrumentation are described by Lee et al. (2014) and Zhang et al. (2020). Here we provide a summary for the reader's convenience (Table 1).

There were seven eddy covariance sites distributed across the lake. One site was located in a habitat of submerged vegetation (ID: BFG), one site was in a lake portion with floating vegetation (ID: DTH), and the other sites were located in open water. Each site was equipped with at least one OPEC system. The operation started in July 2010. As of August 2023, two sites were still active (site ID: BFG, DTH). At BFG, a second OPEC, consisting of a sonic anemometer/ thermometer, an open-path CO_2/H_2O analyzer and an open-path CH_4 analyzer, was in operation from April 2014 to May 2017 (Zhang et al., 2019).

Most of the data presented below came from observations at BFG. At this site, in parallel to the permanent OPEC system, a CPEC system started to measure the CO_2 and the H_2O flux in July 2020. The operation principle of the closed path analyzer (EC155) at BFG is the same as EC150, as described below. It used a "vortex" intake supplied by the EC155 manufacturer to prevent pollutant particles to enter the sample cell of the analyzer. When air passed the vortex intake, particles in the air were centrifuged to the outside of the "vortex filter" and into a bypass line. The clean air passed through the intake tube to reach the sample cell. According to laboratory and outdoor tests, the vortex intake and the analyzer's short intake tube (length 64.5 cm, inner diameter 2.16 mm, stainless steel tube) avoid high-frequency loss and adsorption effect of H_2O by the tube wall (Runkle et al., 2012; Burgon et al., 2016; Ma et al., 2017). The CPEC achieved automatic zero-point calibration and CO_2 span calibration with a calibration frequency of 3 days. The span

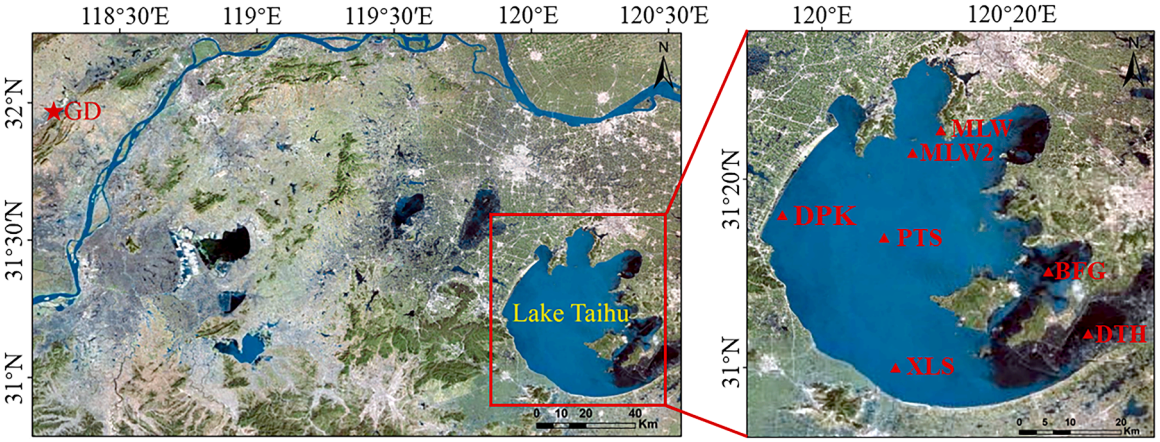

Fig. 1. A satellite image of Lake Taihu Eddy Flux Network and the Guandu land site (GD).

Table 1
Site and instrumentation.

Site ID	Site name	Lat (°N)	Lon (°E)	Biology	EC height (m)	Analyzer type
Lake Sites						
MLW	Meiliangwan	31.420	120.21	Eutrophic	3.5	OPEC[1]
DPK	Dapukou	31.266	119.93	Super eutrophic	8.5	OPEC[1]
BFG	Bifenggang	31.169	120.40	Submerged macrophyte	8.5	OPEC[2] and CPEC[1]
XLS	Xiaoleishan	30.997	120.13	Transitional	9.4	OPEC[2]
PTS	Pingtaishan	31.232	120.11	Mesotrophic	8.5	OPEC[2]
MLW2	Meiliangwan2	31.382	120.16	Eutrophic	6	OPEC[1]
DTH	Dongtaihu	31.061	120.47	Floating Plants	4.5	OPEC[2]
Land Site						
GD	Guandu	31.967	118.26	Cropland	70	OPEC[2] and CPEC[2]

OPEC[1]: LI7500a (LI-COR, Inc., Lincoln, NE, USA).
OPEC[2]: EC150 (Campbell Scientific, Logan, UT, USA).
CPEC[1]: EC155 (Campbell Scientific).
CPEC[2]: TGA200A (Campbell Scientific).

calibration used a standard CO_2 gas with mixing ratio of 400 ppm provided by the National Institute of Metrology, China.

The network used two types of open-path analyzers: EC150 and LI7500 (Table 1). EC150 and LI7500 are non-dispersive mid-infrared gas absorption analyzers. They use a reference wavelength of about 4.0 μm and a measurement wavelength of about 4.3 μm for CO_2 detection. CO_2 absorbs radiation at the measurement wavelength but not at the reference wavelength. After passing through the optical path (about 15 cm in length), the radiation received by the detector of the analyzer is lower than the initial emitted radiation intensity at the measurement wavelength. The initial intensity is determined by the intensity detected at the reference wavelength. The ratio of the two radiation intensities is converted into the CO_2 gas concentration using the Beer-Lambert law.

We used observations at a land site (Guandu; site ID: GD) to compare OPEC and CPEC under different humidity conditions. This site is located at a linear distance of 180 km to the northwest of the lake, in Anhui Province in the YRD. The flux footprint is mainly composed of farmland, with a few isolated forest patches. An OPEC and a CPEC system have been used to measure the CO_2 flux since October 2018 (Table 1; Xie et al., 2022). The OPEC analyzer type is EC150, and the CPEC analyzer type is TGA200A. The cavity of TGA200A is divided into a sample cell and a reference cell. The beam emitted by a laser transmitter is divided into two beams, which enter the sample cell and the reference cell. The reference cell was supplied with a standard gas of known CO_2 molar mixing ratio (15,000 ppm). The attenuation of light due to gas absorption in the cells is detected by the same detector. The TGA200A analyzer also used a vortex intake to filter out particles from the air. A Nafion® tube dryer was used to dry the intake air before it was pumped into the sample cell.

The CO_2 optical signal strength of a gas analyzer, that is, the intensity of radiation at the reference wavelength reaching the receiver, reflects the cleanliness of its optical lens. Deposition of dust and debris and liquid water on the optical window will reduce the optical signal strength, which can impact the gas concentration measurement (Ma et al., 2017). This strength is measured by the intensity of radiation reaching the detector at the reference wavelength. The optical signal strength of EC150 and EC155 ranges from 0 to 1, with 1 indicating that the lens and the light path are completely clean and 0 indicating that the light path is completely blocked. For LI7500, the CO_2 optical signal strength ranges from 0 to 100, with 100 indicating the lens and light path are completely clean and 0 indicating that the light path is completely blocked. In the case of TGA200A, it does not use a reference wavelength and therefore has no signal strength parameter. The EC150 and EC155 signal strengths were recorded at 10 Hz.

In addition to eddy covariance, we also measured the water-air CO_2 flux with the transfer coefficient method at BGF for a short time period (July 12 to September 26 or DOY 194 to 270, 2020). This method requires simultaneous observation of CO_2 concentrations in the surface-layer air and in the water. An equilibrator, following the design of Aho et al. (2021) and McGillis et al. (2001), was used to measure the CO_2 concentration in the water. The equilibrator was a U-shaped PVC pipe, with the longer end sealed and the shorter end open so water could flow out freely. A water pump (Model Mini-Typhoon, Proactive Environmental Products International LLC, Bradenton, FL, USA) drew water from 20 to 30 cm below the lake surface and pushed it through a union connector at the top of the sealed end of the equilibrator. The water came down in small diffuse droplets through a sprinkler. By spraying, the air in the headspace was brought into equilibrium with the water. The CO_2 concentration of headspace was measured using a non-dispersive infrared CO_2 analyzer (Model Licor 840, LiCor Inc., Lincoln, NE, USA). The temperature of water in the chamber was measured with a chain of temperature probes (Model 109-L, Campbell Scientific, Logan, UT, USA).

2.2. Data processing

For OPEC, the CO_2 flux was calculated using the EddyPro software (Version 6.2.1, LI-COR Inc, Lincoln, NE, USA) from the 10 Hz raw data. A double coordinate rotation was performed to make the half-hour mean vertical and lateral velocity components equal to zero. The WPL density correction was applied to eliminate the density effects of heat and water vapor (Webb et al., 1980). An additional correction for a spectral effect on EC150 analyzers was performed using the method described by Helbig et al. (2016).

For the CPEC with EC155, the half-hourly CO_2 flux was calculated using the EasyFlux® DL CR6 CP program installed in its data logger. Raw time series data were filtered using sonic and gas analyzer diagnostic codes, as well as signal strength and measurement output range thresholds. A double coordinate rotation was used. The lag time of the CO_2 measurement relative to sonic wind measurements was determined via maximization of the CO_2 and vertical wind covariance (Horst and Lenschow, 2009; Foken et al., 2012). A typical lag time was 0.1 to 0.4 s. The analyzer expressed the CO_2 concentration as the dry molar mixing ratio, and the sampling tube eliminated temperature fluctuations, so no WPL correction for temperature is required.

For the CPEC with TGA200A, the half-hourly flux was determined with the EddyPro software from the 10 Hz data. The time lag between CO_2 and the vertical velocity was also determined via covariance maximization. A typical lag time was 7.4 s. No density corrections were applied as the air was dried prior to the concentration measurement. A double coordinate rotation was also applied to the 30-min flux data.

The transfer coefficient method determines the CO_2 flux using the water-air concentration difference and the gas transfer rate between water and the atmosphere (Cole and Caraco, 1998):

$$F = k\left(C_w - C_{\mathrm{eq}}\right)$$

where F is the CO_2 flux, C_{eq} is the concentration of CO_2 in equilibrium with the atmosphere, C_w is the actual concentration of CO_2 in the water, and k is the transfer coefficient of CO_2 at the water-air interface. The transfer coefficient was calculated according to the model established by Cole and Caraco (1998). The CO_2 concentration observed with CPEC was used to determine C_{eq} in conjunction of the Henry coefficient for CO_2.

3. Results

3.1. Negative nocturnal CO_2 flux at lake sites

Negative CO_2 flux was frequently observed during nighttime at the lake sites. In the example given in Fig. 2a, the flux showed similar and significant periodic diurnal variations at all the active sites during a 10-day period in 2018 (March 25 to April 4 or DOY 84 to 94). The negative CO_2 flux usually persisted through the whole evening, with nearly identical phase and magnitude across the lake. The flux magnitude was small in the daytime (mean value -0.89 μmol m^{-2} s^{-1} from 6:30 to 18:00 local time), increased rapidly after sunset, and reached the peak the next morning between 04:30 and 06:30 local time. The most negative flux during this period (-20.6 μmol m^{-2} s^{-1}) was recorded at PTS in the middle of the lake at 05:00 on 31 March (DOY 90). These negative flux values give the impression of CO_2 uptake by the lake, as if the lake were removing a large amount of CO_2 from the atmosphere at night.

The second example, shown in Fig. 2b, was observed from July 23 to August 1 (DOY 205 to 215), 2012, in the early stage of the flux network when three sites (MLW, BFG and DPK) were operational. The wind was from the east. The nocturnal negative flux did not occur at MLW. The diurnal variation shown in Fig. 2b is typical at MLW when the easterly winds dominated, presumably because the site, being only 200 m from the shore, was heavily influenced by the respiration flux of land vegetation. The other two sites (BFG and DPK) had sufficient fetch (Fig. 1), and both showed persistently negative flux at night. The most negative flux during this period was -22.1 μmol m^{-2} s^{-1}, observed at BFG between 22:30 and 23:00 on 31 July (DOY 213). The reader is reminded that the CO_2 gas analyzers were different at BFG (EC150) and at DPK (LI7500). This event indicates that OPEC has inherent design issues that are unrelated to the type of instrument used.

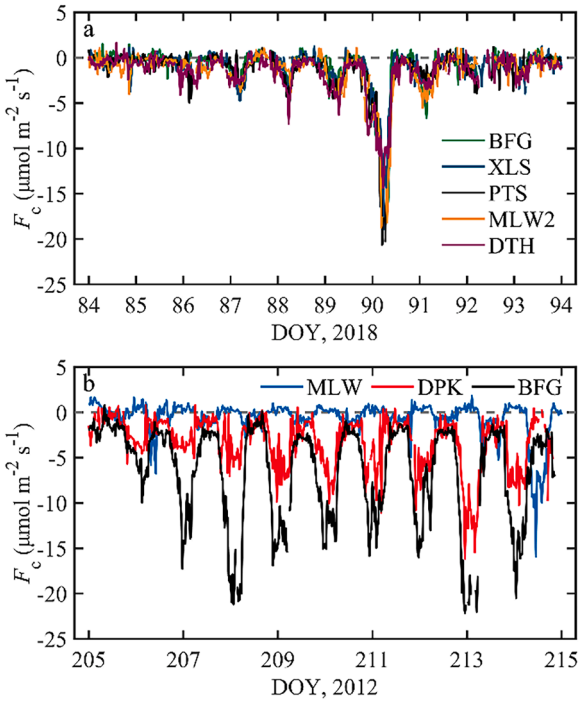

Fig. 2. (a) Half-hourly OPEC CO_2 flux time series during a 10-day period from March 25 to April 4, 2018, at five sites across Lake Taihu. (b) Half-hourly OPEC CO_2 flux time series during a 10-day period from July 23 to August 1, 2012 at three lake sites.

At BFG, the longest running site of the network, we observed, on average, 11 persistent nocturnal negative flux events per year between 2012 and 2022. Table S1 summarizes the event number for other lake sites. Here a persistent negative flux event is defined as two or more consecutive nights that experienced a negative flux with magnitude greater than 2 μmol m^{-2} s^{-1}. Some of these persistent events lasted more than five days. Negative flux events with durations shorter than 12 h were much more numerous.

3.2. Comparison with closed-path eddy covariance

Fig.3a shows time series of the half-hourly CO_2 flux observed with the OPEC and CPEC systems at the BFG lake site during a typical 10-day period (August 15 to August 25, 2020). The same data are also shown in a 1:1 comparison (Fig. 3b) and as diurnal composites (Supplementary Fig. S1). The nocturnal negative flux measured with the OPEC system was quite strong. The diurnal composite flux reached the most negative value of -6.7 μmol m^{-2} s^{-1} at midnight, with the 24-h mean value of -3.3 μmol m^{-2} s^{-1}. In comparison, the half-hourly CPEC flux fluctuated only slightly around zero, showing no obvious diurnal pattern. The mean CPEC flux was $+0.1$ μmol m^{-2} s^{-1}. There is no correlation between the two systems (Fig. 3b).

The two analyzers used the same absorption and reference wavelengths for detection, but they differed in two important respects. First, the density effect was larger for the OPEC system than for the CPEC system. The mean sensible and latent heat flux were 14.5 W m^{-2} and 139.6 W m^{-2} at midnight during this period. The corresponding density corrections on the OPEC flux were $+0.8$ μmol m^{-2} s^{-1} and $+1.2$ μmol m^{-2} s^{-1}, giving a total correction of about $+2.0$ μmol m^{-2} s^{-1} (Supplementary Fig. S2). In the case of the CPEC measurement, there was no density effect associated with temperature fluctuations, so only the water vapor density effect needed correction. Second, the OPEC analyzer was influenced by aerosol particles in the air, but the CPEC analyzer was not. We will return to this point later in Section 4.

3.3. Comparison with the transfer coefficient method

Fig. 4 compares the flux measured with the OPEC and CPEC systems with that measured with the transfer coefficient method at the BFG site from July 30 to August 6, 2020. During this time, all three systems were functioning properly. The OPEC flux varied from –13.6 to +0.7 μmol m^{-2} s^{-1}, with diurnal variation characteristics similar to those described above. The mean daytime (6:00 to 19:00), nighttime (20:00 to 5:00) and 24-h flux were –1.3 μmol m^{-2} s^{-1}, –3.0 μmol m^{-2} s^{-1} and –1.9 μmol m^{-2} s^{-1}, respectively. The CPEC flux varied from –2.7 to +1.4 μmol m^{-2} s^{-1}; Its mean daytime, nighttime and 24-h value were +0.08 μmol m^{-2} s^{-1}, +0.03 μmol m^{-2} s^{-1} and +0.06 μmol m^{-2} s^{-1}, respectively. The CO_2 flux observed with the transfer coefficient method varied from –0.01 to +0.01 μmol m^{-2} s^{-1}, with the mean daytime, nighttime and 24-h flux of –0.003 μmol m^{-2} s^{-1}, –0.004 and –0.003 μmol m^{-2} s^{-1}, respectively. The CO_2 flux with the transfer coefficient method is one order of magnitude smaller than the CPEC flux. The reason for this difference may be that the CPEC observation represented the average CO_2 flux within a large footprint area, while the transfer coefficient method only observed the CO_2 exchange at the water-air interface and at a single point. During this observation period, some of the submerged plant leaves had emerged to the water surface and could directly exchange CO_2 with the atmosphere (Watanabe and Kuwae, 2015). The measurements by the CPEC and the transfer coefficient method did not show large nocturnal CO_2 uptake by the lake. Moreover, the concentration of CO_2 in the water column gradually increased with time at night, which

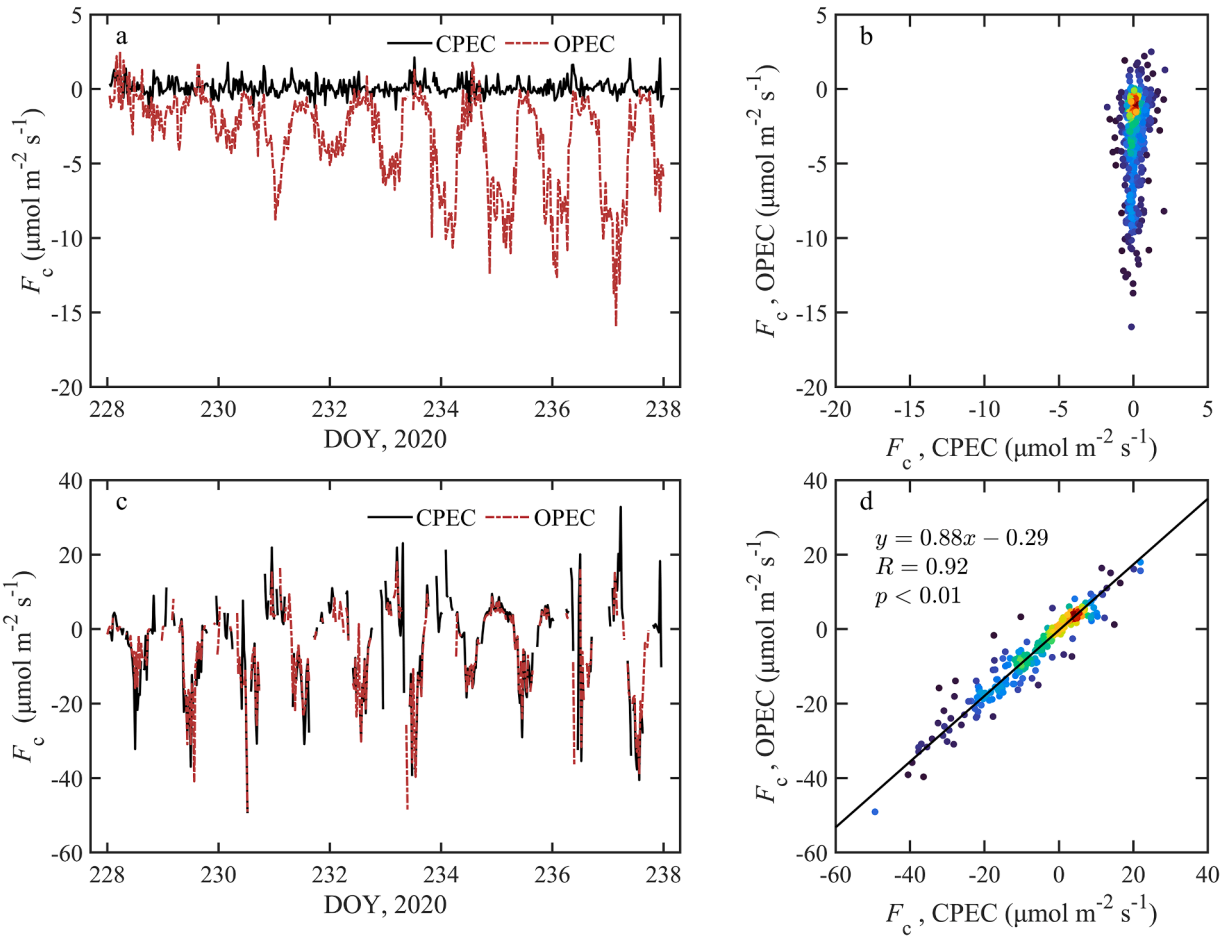

Fig. 3. Comparison of the CO_2 flux observed with OPEC and CPEC systems at the BFG lake site (a & b) and at the GD land site (c & d), from August 15 to August 25, 2020. Colors in the scatter plots (panels b and d) indicate data density.

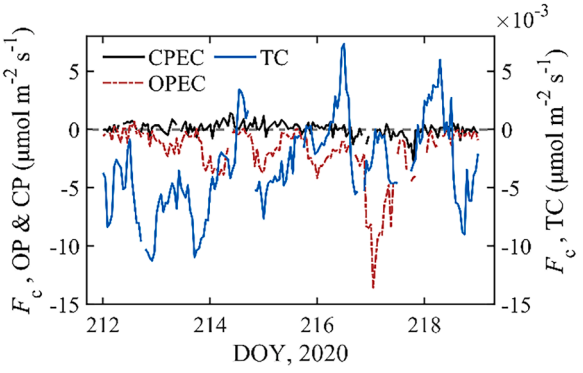

Fig. 4. Hourly CO_2 flux observed with three methods at the BFG lake site from July 30 to August 6, 2020. OPEC: open-path system; CPEC: closed-path system; TC: transfer coefficient method.

contradicts the nocturnal negative CO_2 flux (Fig. S8). A logical conclusion is that the nocturnal CO_2 absorption phenomenon observed with the OPEC was a false signal unrelated to biological processes.

3.4. Interference with OPEC optical signal strength

Fig. 5 shows a 10 Hz time series of the vertical velocity (w), the CO_2 signal strength (s) and the dry CO_2 molar mixing ratio (r_c) measured with the OPEC and CPEC systems at BFG for a duration of 5 min (from 23:55 to 24:00) on August 18, 2020. The OPCE and CPEC fluxes were –5.1 μmol m^{-2} s^{-1} and –0.1 μmol m^{-2} s^{-1} for the corresponding half-hour period (23:30 to 24:00; Fig 3). The vertical velocity fluctuations showed good agreement between the two systems. But in comparison with the stable s of the CPEC system, the s of the OPEC was highly variable at the 10 Hz frequency. Likewise, the r_c of CPEC was stable, but the r_c of OPEC showed large fluctuations. The mean r_c of OPEC during this 5-min period (414.2 ppm) was lower than the mean r_c of CPEC (436.3 ppm). The mean s was 0.940 and 0.844 for the CPEC and OPEC system, respectively. The reduction in the mean of s indicates that the optical path of the OPEC was partially blocked.

The s and r_c of OPEC were positively correlated with each other at 10 Hz. Their covariance was 2.6×10^{-3} μmol^{-1} for the 5-min time series shown in Fig 5. Both s and r_c were negatively correlated with the vertical velocity ($\overline{w's'} = -2.0 \times 10^{-4}$ m s^{-1} and $\overline{w'r_c'} = -0.15$ μmol^{-1} m s^{-1}).

Fig. S9 is a scatter plot of the 30-min flux versus the correlation coefficient between the CO_2 concentration and the signal strength, calculated using the 10 Hz data, for the 10-day period covered by Fig. 3 (August 15 to August 25, 2020). For OPEC, when the CO_2 flux was below −5 μmol m^{-2} s^{-1}, the correlation was greater than 0.8; when the CO_2 flux was greater than −1 μmol m^{-2} s^{-1}, the correlation coefficient approached 0 (Fig. S9a). For CPEC, there is no obvious relationship between the correlation coefficient and the CO_2 flux (Fig. S9b). Moreover, for OPEC, both the standard deviation of r_c and that of the signal strength increased when the CO_2 flux became more negative (Fig. S10a). There is a linear relationship between these two standard deviations, especially when the CO_2 flux was below −5 μmol m^{-2} s^{-1}. These results indicate that the fluctuation of the CO_2 concentration was greatly affected by the fluctuation of the signal strength.

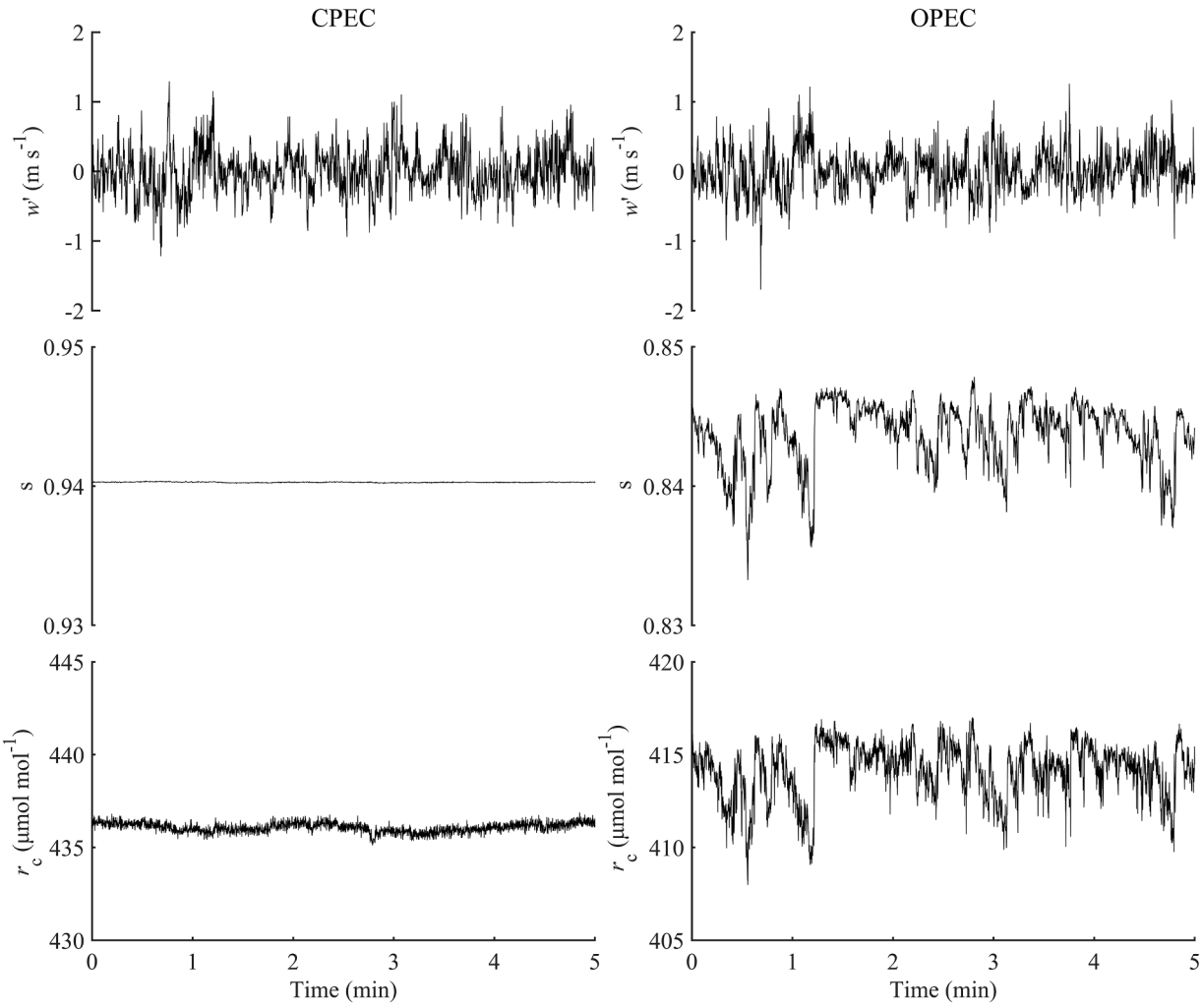

Fig. 5. 10-Hz time series of the vertical air velocity fluctuation (w'), the CO_2 signal strength (s) and CO_2 molar mixing ratio (r_c) observed at the BFG lake site between 23:55 and 24:00 on August 18, 2020. Left panels: CPEC; right panels: OPEC.

Three inferences can be made from these correlation patterns. First, the interference was variable at time scales of eddy motion. Second, the interfering substance impacted light attenuation differently at the absorption and at the reference wavelength. The true r_c in the atmosphere did not show clear fluctuation patterns according to the CPEC system. If the interference were equal at these two wavelengths, the relative absorption would not change over time, and hence the measured concentration would not fluctuate. Third, the interfering substance caused a greater attenuation at the reference wavelength than at the absorption wavelength so as to produce a positive correlation between s and r_c. We know this because the measured r_c is inversely related to the ratio of the strength of light received by the optical detector at the absorption wavelength to that at the reference wavelength. The optical reason as to why the interference was greater at the reference wavelength than at the absorption wavelength remains unknown.

3.5. Comparison between OPEC and CPEC at the land site

At the land site (site ID: GD), the CO_2 flux measured with an OPEC and a CPEC system showed virtually no difference. An example is given in Fig. 3b for the period from August 15 to August 25, 2020. In the same period, the OPEC flux at the BFG lake site displayed strongly negative CO_2 flux at night as described earlier (Fig. 3a). The mean OPEC and CPEC flux at GD were –5.7 and –6.1 μmol m^{-2} s^{-1}, respectively during the period shown in Fig. 3c. Both showed CO_2 absorption during the daytime and emission during the nighttime, and were highly correlated with a linear correlation of 0.92 (Fig. 3d).

The open-path analyzer at GD was the same type used at the BFG lake site. The 30-min s was about 0.9 and showed small day-to-day variations (Supplementary Fig. S3). The 30-min r_c of OPEC was biased low by about 16.1 ppm, but it followed the diurnal and the day-to-day variations of the r_c of CPEC nearly perfectly (R^2 = 0.95; Supplementary Fig. 4). Supplementary Fig. S5 is a 10-Hz time series plot of s, r_c and w of the OPEC and the CPEC system for a five min period from 05:00 to 05:05 on August 19, 2020. The corresponding half-hourly (05:00 to 05:30; Supplementary Fig S3) mean s was 0.879, the lowest during the period shown in Fig. 3 (August 15 to August 25, 2020). The 10 Hz fluctuations in s were two orders of magnitude smaller (Supplementary Fig. S5) than those seen at the BFG lake site (Fig. 5). The covariance $\overline{w's'}$ was also two orders of magnitude smaller.

The cropland was a large source of CO_2 at night due to soil and plant respiration. It is possible that the OPEC flux had a negative bias, but the bias was masked by the large ecosystem respiration signal. To rule out this possibility, in Supplementary Fig. S6 we show the diurnal composite of the flux difference between the OPEC and CPEC for the whole year of 2019. There is a small difference of about –0.7 μmol m^{-2} s^{-1} between the two systems, but the difference has no diurnal pattern. Had the OPEC flux had a negative bias at night, the flux difference would be more negative at night than during the day.

4. Discussion

4.1. Potential mechanisms

4.1.1. Crassulacean acid metabolism (CAM)

Several mechanisms exist that can potentially explain the large negative flux at night. We offer a brief discussion on each. In the early phase of the Taihu Eddy Flux Network, we thought that the negative flux was indicative of the Crassulacean Acid Metabolism (CAM) mechanism (Lee et al., 2014). The negative nighttime eddy flux has been shown for a CAM ecosystem on land (Owen et al., 2016). In the eddy flux footprint at BFG, the main macrophyte species were *Potamogeton malaianus* and *Hydrilla verticillata*, two species known to deploy CAM for carbon capture (Holaday and Bowes, 1980; Yin et al., 2017). We made ^{13}C isotope measurement of four stem samples (two for each of *Potamogeton malaianus* and *Hydrilla verticillata*) collected in November 2012. The analysis was performed on a stable isotope mass spectrometer (model MAT253 with Flash 2000, Thermo Finnigan) against standards traceable to the IAEA-CH-6 scale of the International Atomic Energy Agency. The mean $\delta^{13}C$ of these samples was –14.7 ± 1.2 ‰ (VPDB scale, mean ± 1 standard deviation), which is closer to the isotopic signature of CAM plants than to that of C_3 plants (Griffiths, 1992; Winter et al., 2002). However, with additional observations we now rule out this mechanism. First, the water equilibrium method and the CPEC did not observe obvious CO_2 absorption at BFG at night (Fig. 4). Second, the negative CO_2 flux (with OPEC) also occurred at other open water sites without submerged plants (Fig. 2a). Third, the peak magnitude of the negative flux shown in Figs 2a and 2b is unlikely to be biological origin as it is 2 times larger than the nighttime uptake flux of a CAM ecosystem on land (Owen et al., 2016). The high $\delta^{13}C$ of the plant biomass at BFG may have been caused by the utilization of bicarbonate as the source of carbon for photosynthesis because bicarbonate is more enriched in ^{13}C than atmospheric CO_2 due to a chemical fractionation effect (Mook et al., 1974).

4.1.2. Density effects

Density effects associated with fluctuations in temperature and humidity are known to cause negative CO_2 flux. Fig. S2 displays diurnal composites of the raw CO_2 flux, the WPL-corrected CO_2 flux, and the CO_2 flux with an additional correction for a spectroscopic effect on EC150 analyzers (Helbig et al., 2016), for the OPEC system at BFG during August 15 to August 25, 2020. The largest WPL correction was 2.1 μmol m^{-2} s^{-1} at 22:00. The CO_2 flux at this time was –7.3 and –5.2 μmol m^{-2} s^{-1} before and after the WPL correction. In other words, the WPL correction did not eliminate the negative flux. For the sake of argument, to correct a flux of –5.2 μmol m^{-2} s^{-1} to zero, we would need an additional sensitive heat flux of +113 W m^{-2}. If the most negative flux (–22.1 μmol m^{-2} s^{-1}) in Fig. 2b were caused by the density effect due to temperature fluctuations, we would need an additional sensible heat flux of +477 W m^{-2}. Sensible heat fluxes of these magnitudes is impossible at night as it would violate the energy balance constraint.

4.1.3. Self-heating

Self-heating can cause negative CO_2 flux observed with OPEC. Heating of the instrument itself and additional heat of the sensor head by solar radiation can cause the temperature in the sensor optical path to fluctuate more than the ambient temperature, resulting in unreasonable CO_2 flux values. The self-heating effect is evident during the nongrowing season in cold environments (Burba et al., 2006a, b; Amiro et al., 2010; Grelle and Burba, 2007; Ono et al., 2008; Haslwanter et al., 2009; Wang et al., 2016). This effect typically manifests as a negative flux during midday, presumably because solar heating of the sensor is the strongest. EC150 open-path analyzers are equipped with a window heater. In the present study, this heater was disabled except for the brief test described below. Unlike the studies in dryland systems, in the present study the abnormal negative CO_2 flux occurred at night and is therefore not related to solar heating. On the contrary, due to the emission of longwave radiation at night, temperature fluctuations of the sensor head may have a reverse effect on the CO_2 flux.

4.1.4. Condensation

For OPEC, it is crucial to keep the gas analyzer's optical lens clean of liquid water. If rain or dew completely covers the sensor lens, the infrared light emitted by the sensor will be blocked, resulting in data loss. If the windows are covered by a thin film of dew, its transmittance at the absorption wavelength may differ from that at the reference wavelength, resulting in errors in the observation of the CO_2 concentration. As mentioned earlier, if the temperature of the sensor head is lower than the ambient temperature at night, water vapor can condense on the instrument surface, forming a thin dew layer (Heusinkveld et al., 2008).

In the example shown in Fig. 3, the mean nighttime air temperature was 30.14 °C, and the mean dewpoint temperature was about 4 °C lower, at 25.99 °C (Fig. S7). Burba et al. (2008) reported that the temperature of their sensor head is about 1 °C lower than the ambient temperature at night, due to the emission of longwave radiation. Although we did not measure the temperature of the EC150 optical lens, we observed that the temperature of the net radiometer, which was made of similar material and coating as the EC150 shell, was only 0.3 °C lower than the air temperature at night. In other words, the sensor head temperature after accounting for radiative cooling should have exceeded the dewpoint temperature by more than 3 °C, which makes condensation on the optical window very unlikely.

To further rule out the condensation effect, we turned on the lens heater for a short period of time (April 26 to May 19 or DOY 116 to 139) in 2021. Fig. 6 shows a 24-h data sample from this test period. An event of negative OPEC CO_2 flux was evident at night, and the OPEC concentration was lower than the CPEC concentration. Despite heating, the signal strength *s* of OPEC was as low as 0.83, indicating partial blockage. The highest relative humidity in the atmosphere was 75 %. We can rule out condensation during this negative flux episode because the relative humidity in reference to the sensor head temperature should be lower than 75 % due to sensor heating.

4.1.5. Aerosol interference

Aerosol interference is the most logical explanation of the negative flux observed with OPEC. At the BFG lake site, the OPEC and CPEC systems used identical optical sensors for detection. The biggest difference is that air in the CPEC's optical path was free of particulate matter but air in the OPEC's optical path was not. However, the reduction in the *s* of OPEC was too large to be caused by aerosols floating in the optical path which is only 15.37 cm long; Instead, it must have been caused by blockage of particles accumulated on the optical lens. In theory, use of dual wavelengths should eliminate observation errors caused by a dirty optical window. In practice, some residual errors may still exist, in the form of an offset in the mean CO_2 concentration or a slight reduction in the sensitivity of the analyzer (Kondo et al., 2014), but the blockage itself should not amplify the flux signal or cause it to change sign.

Here we propose that during the episodes of persistent negative flux, particles deposited on the optical lens changed the cross-sensitivity caused by water vapor, to the extent that the manufacturer's default correction factor no longer worked. The cross sensitivity here refers to the additional CO_2 fluctuations caused by refraction and scattering of light by water vapor molecules at the CO_2 measurement and the reference wavelengths. Water vapor has a higher refractive index at the reference wavelength, resulting in more optical signal loss at the reference wavelength than that at the measurement wavelength. A decrease in the optical signal at the reference wavelength can lead to an underestimation of the CO_2 concentration (Kohsiek 2000). In high humidity environments, hygroscopic aerosols promote the formation of tiny droplets on the optical lens. When this occurs, the cross sensitivity may be increased. As a result, light transmission at the reference wavelength

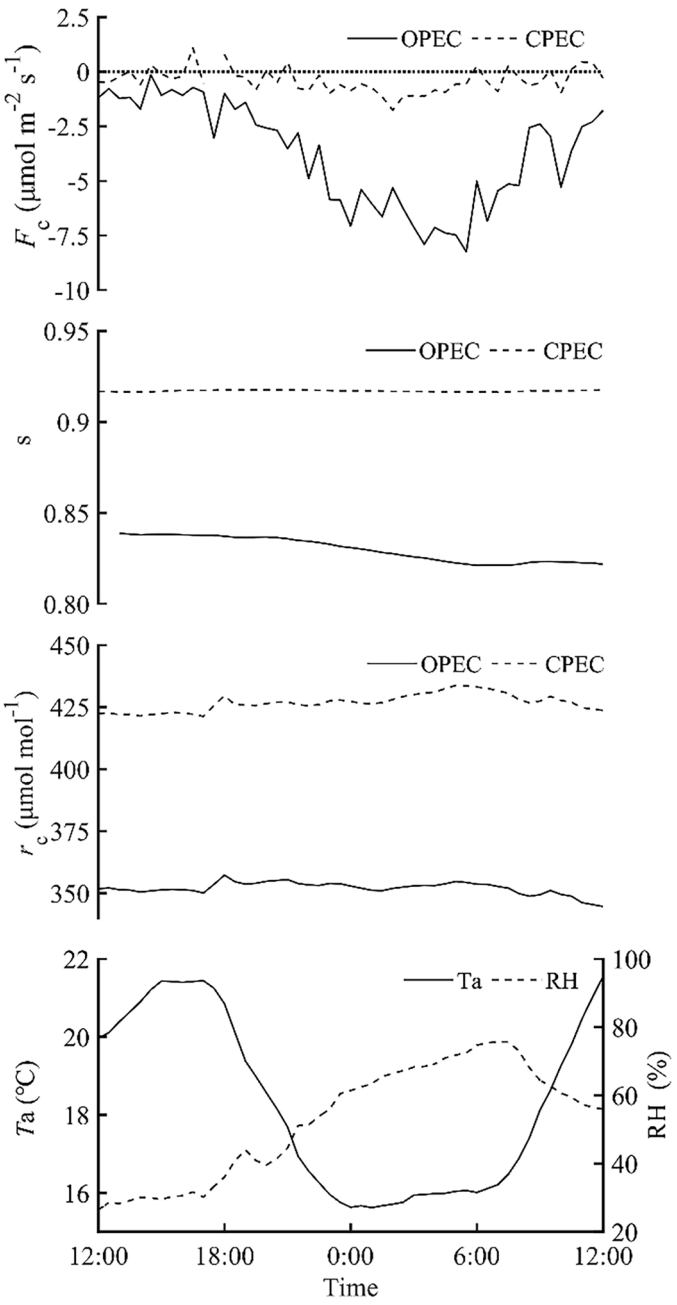

Fig. 6. Half-hourly CO_2 flux (F_c), CO_2 signal strength (s), CO_2 concentration (r_c), air temperature (T_a) and relative humidity (RH) at the BFG lake site from May 2 to 3, 2021. In this period, the optical lens heater was turned on.

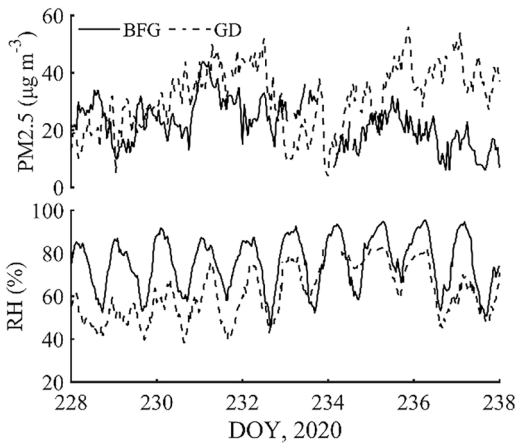

Fig. 7. PM2.5 concentration observed near the BFG lake and the GD land site and relative humidity observed at these sites from August 15 to 25, 2020. PM2.5 data were obtained at sites about 35 km away from GD and about 20 km away from BFG.

became extremely sensitive to fluctuations in the water vapor concentration within the optical path. Evidence of this interference has been reported for the marine environment (Prytherch et al., 2010; Nilsson et al., 2018). Prytherch et al. (2010) observed a negative correlation between CO_2 and humidity fluctuations at 20 Hz. This correlation caused an apparent downward CO_2 flux of –2.8 μmol m^{-2} s^{-1} to the ocean surface, which is an order of magnitude larger than expected of the conditions at the time of their observation. They suggest that this effect is caused by hygroscopic salt particles accumulated on their optical lens. Our observation can be interpreted similarly. Our lake sites were heavily influenced by urban pollution. During the period shown in Fig. 3 (August 15 to August 25, 2020), the PM2.5 concentration varied between 6 and 44 μg m^{-3} at a site near BFG (Fig. 7). In year 2022, the annual mean PM2.5 concentration was 28 μg m^{-3} in Suzhou, a city at a distance of 20 km from BFG. According to Cui et al. (2023), about 50 % of PM2.5 in the Yangtze River Delta region are sulfate and nitrate salts and soluble organic matter. These particles are hygroscopic. They gradually accumulated on the optical window during fair weather days. They grew hygroscopically in high humidity conditions at night and dried out during the day, as suggested by the lower CO_2 signal strength at night than during the day (Fig. 8). That abnormal negative flux rarely occurred during the day indicates that these particles in dry state did not interfere with the instrument's cross sensitivity to water vapor.

At the GD land site, the CO_2 flux observed with OPEC and CPEC showed virtually no difference. The PM2.5 concentration at the land site was similar to that at the lake site (Fig. 7 top panel). Two reasons can explain why the OPEC system at GD was unaffected by aerosols. First, relative humidity in the atmosphere at the land site was generally lower than that at the lake site (Fig. 7 bottom panel). The low s value (e.g., 0.88, Fig. S3) indicates that there were particles on the OPEC's optical lens, but the low humidity condition may have limited their hygroscopic growth. Indeed, the diurnal variation in its s (Fig. S3) was 5 to 10 times weaker than that observed at the BFG lake site (Fig. 8). The aerosol interference at GD was primarily an effect of blockage, which caused the OPEC concentration to be lower by an offset of about 18 ppm than the CPEC concentration, but it did not change the OPEC sensitivity appreciably (slope of regression = 0.92; Fig. S4). Second, we expect weak turbulent fluctuations in the water vapor concentration at GD at night owing to low nighttime evaporation on land. In Fig. 5, we showed the turbulent time series of w, s and r_c for the BFG lake site; the corresponding half-hourly latent heat flux was 180.8 W m^{-2}. In comparison, the half-hourly flux for the land example shown in Fig. S5 was only 6.7 W m^{-2}. On the annual time scale, the latent heat flux on land is about 8 W m^{-2} at night, which is an order of magnitude smaller than the lake latent heat flux (Wang et al., 2014). Even if the cross-sensitivity to water vapor were equally affected by aerosols, the OPEC at the land site would still suffer much smaller errors due to weaker interference of water vapor fluctuations with the reference signal than at the lake site.

4.2. *Correcting the aerosol interference*

Prytherch et al. (2010) proposed a post-processing method, termed the PKT method, to correct the optical window contamination. PTK is an iterative routine that adjusts the dependence of the observed high frequency CO_2 concentration on relative humidity. This procedure reduces their flux by an order of magnitude. However, in a subsequent observation over the ocean, Landwehr et al. (2014) showed that PKT produces erroneous results. Huang et al. (2012) found that the PKT method may

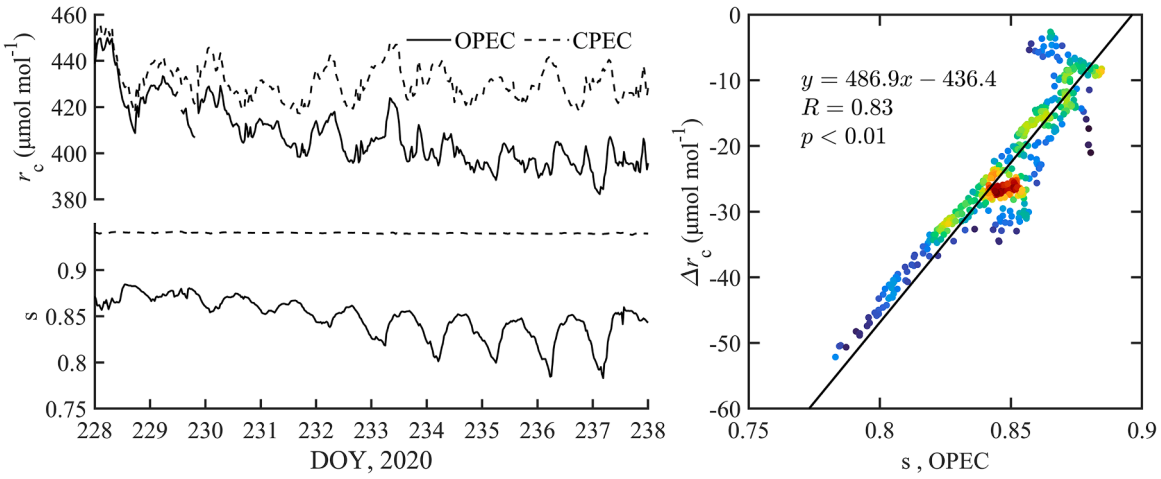

Fig. 8. Left panels: Half-hourly CO_2 concentration (r_c) and signal strength (s) measured with OPEC and CPEC at the BFG lake site; Right panel: relationship between CO_2 concentration difference Δr_c (OPEC minus CPEC) and OPEC s. Colors indicate data density.

result in over-correction when the latent heat flux is small.

In the present study, the reference signal strength was recorded at the same sampling frequency (10 Hz) as the vertical velocity w. Here we attempted to correct the cross-sensitivity to water vapor using $\overline{w's'}$, the covariance between w and s. We used the CO_2 flux observed with CPEC as the standard, and the difference between the CO_2 flux observed with OPEC and CPEC (ΔF_c; OPEC minus CPEC) is observation error. Using the data given in Fig 3a, we found a robust linear relationship (linear correlation $R = 0.71$) between ΔF_c and $\overline{w's'}$ (Fig. 9). According to this relationship, the true flux $F_{c,\ corrected}$ (μmol m^{-2} s^{-1}) is related to the measured flux F_c (μmol m^{-2} s^{-1}) as:

$$F_{c,\ corrected} = F_c - 1.73 \times 10^4 \times \overline{w's'} + 0.4$$

We then applied this correction to the OPEC flux. After this correction, the OPEC flux was much smaller in magnitude (Fig. 10). The daily average CO_2 flux after correction was + 0.067 μmol m^{-2} s^{-1}, which is similar to the CO_2 flux observed with CPEC (+ 0.077 μmol m^{-2} s^{-1}). After this correction, about 90 % of the half-hourly observations fall in the range of ±2 μmol m^{-2} s^{-1}. However, the flux was still quite negative

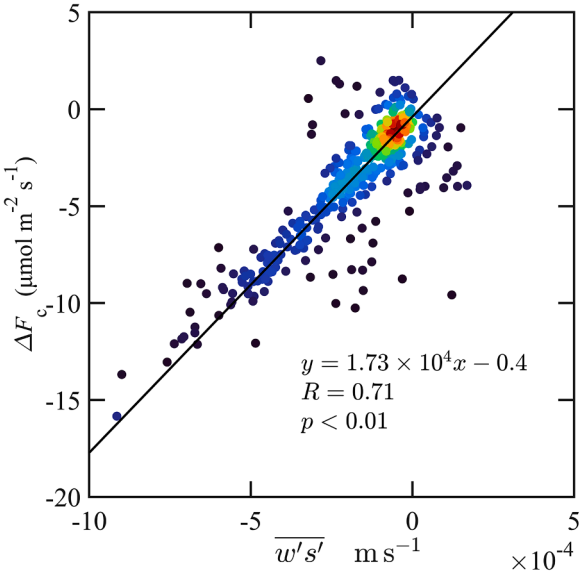

Fig. 9. Relationship between the CO_2 flux difference ΔF_c (OPEC minus CPEC) and $\overline{w's'}$ (covariance between CO_2 signal strength and vertical velocity). Data are for the BFG lake site from the period shown in Fig. 8.

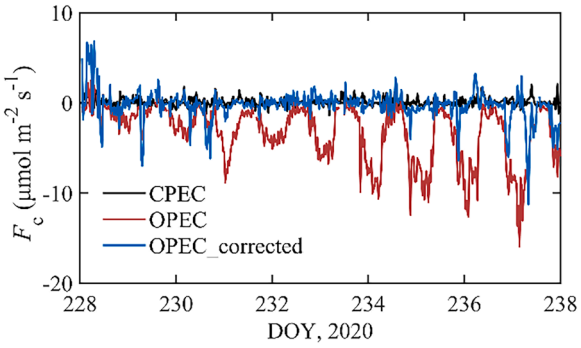

Fig. 10. Half-hourly CO_2 flux observed with OPEC and CPEC at the BFG lake site and the corrected OPEC CO_2 flux.

for several short morning and evening transitional periods (e.g., between 6:30 and 9:00, DOY 237). During these periods, the contaminant on the optical lens might be undergoing rapid hydration or dehydration phase, and the cross-sensitivity to water vapor itself might be changing rapidly.

5. Conclusions

In this study, we performed detailed analysis of the CO_2 flux observed with an OPEC system, a CPEC system and the TC method at a lake site (BFG) and the flux observed with an OPEC system and a CPEC at a land site (GD). Located in the highly industrialized Yangtze River Delta, these sites were influenced heavily by aerosol pollution. The key results are summarized as follow:

1) The persistent negative nighttime CO_2 flux observed with OPEC at BFG and other lake sites was a measurement artifact, unrelated to biological processes such as the Crassulacean Acid Metabolism. Density effects, sensor self-heating and condensation cannot reasonably explain this large negative CO_2 flux at night.
2) There is strong evidence that particles deposited on the optical lens of the OPEC analyzer changed the cross-sensitivity to water vapor, to the extent that the manufacturer's default correction factor no longer worked. A possible mechanism is that these particles were hygroscopic; they grew at night when humidity was high, causing interference with the light transmission at the reference wavelength of the analyzer. The problem was made more severe by the high lake water vapor flux at night.

3) The signal strength of the OPEC analyzer at BFG showed large fluctuations at 10 Hz during periods when the flux was negative. These fluctuations were positively correlated with the 10 Hz CO_2 concentration time series. The positive correlation implies that the interfering substance caused a greater attenuation at the reference wavelength than at the absorption wavelength of the analyzer.
4) The half-hourly CO_2 flux difference (OPEC minus CPEC) at BFG was highly correlated with the half-hourly $\overline{w's'}$ (covariance between the signal strength and vertical velocity). We suggest that this linear correlation can be used to perform post-field correction of the OPEC flux data.
5) Aerosol interference was not detectable at the GD land site. The flux difference between the OPEC and the CPEC at GD did not show an obvious diurnal pattern. Although the half-hourly mean signal strength of the OPEC analyzer indicated partial blockage of its optical window at times, there was no correlation between its signal strength and the concentration at 10 Hz. Possible reasons included lack of hygroscopic growth of particles on the optical window and weak water vapor flux at night.

CRediT authorship contribution statement

Lei Jia: Writing – original draft, Methodology, Investigation, Formal analysis. **Mi Zhang:** Writing – original draft, Methodology, Formal analysis. **Wei Xiao:** Methodology, Funding acquisition, Data curation. **Yini Pu:** Data curation. **Zhen Zhang:** Data curation. **Hengxin Bao:** Data curation. **Pei Ge:** Data curation. **Jie Shi:** Data curation. **Yang He:** Data curation. **Fuyu Yang:** Data curation. **Kelly Aho:** Methodology. **Peter Raymond:** Methodology. **Xuhui Lee:** Writing – review & editing, Conceptualization.

Declaration of competing interest

The authors declare no conflict of interest.

Data availability

Data will be made available on request.

Acknowledgements

This study was supported by the National Natural Science Foundation of China (42021004 & 41975143 to WX), the R&D Foundation of Jiangsu Province, China (BK20220020 to WX), the National Key R&D Program of China (2020YFA0607501 to WX), the Natural Science Foundation of Jiangsu Province for Distinguished Young Scholars (BK20220055 to WX), the "333 Project" of Jiangsu Province (BRA2022023 to WX), and the Postgraduate Research & Practice Innovation Program of Jiangsu Province (KYCX23_1321 to LJ). We acknowledge helpful discussions with George Burba and Ivan Bogoev on this topic.

Supplementary materials

Supplementary material associated with this article can be found, in the online version, at doi:10.1016/j.agrformet.2024.110104.

References

Aho, K.S., Hosen, J.D., Logozzo, L.A., McGillis, W.R., Raymond, P.A., 2021. Highest rates of gross primary productivity maintained despite CO_2 depletion in a temperate river network. Limnol. Oceanogr. Lett. 6, 200–206. https://doi.org/10.1002/lol2.10195.

Amiro, B., 2010. Estimating annual carbon dioxide eddy fluxes using open-path analysers for cold forest sites. Agric. For. Meteorol. 150, 1366–1372. https://doi.org/10.1016/j.agrformet.2010.06.007.

Blomquist, B.W., Huebert, B.J., Fairall, C.W., Bariteau, L., Edson, J.B., Hare, J.E., McGillis, W.R., 2014. Advances in air–sea CO_2 flux measurement by eddy correlation. Boundary-Layer Meteorol 152, 245–276. https://doi.org/10.1007/s10546-014-9926-2.

Burba, G.G., Anderson, D.J., Xu, L., McDermitt, D.K., 2006a. Correcting apparent off-season CO_2 uptake due to surface heating of an open path gas analyzer: progress report of an ongoing study. In: Proceedings of the 27th annual conference of agricultural and forest meteorology. San Diego, CA, pp. 1–13.

Burba, G.G., Anderson, D.J., Xu, L., McDermitt, D.K., 2006b. Additional term in the Webb-Pearman-Leuning correction due to surface heating from an open-path gas analyzer. AGU Fall Meet. Abstr. 2006, C12A–C103.

Burba, G.G., McDERMITT, D.K., Grelle, A., Anderson, D.J., Xu, L., 2008. Addressing the influence of instrument surface heat exchange on the measurements of CO_2 flux from open-path gas analyzers. Glob. Chang. Biol. 14, 1854–1876. https://doi.org/10.1111/j.1365-2486.2008.01606.x.

Burba, G., Anderson, T., Komissarov, A., 2019. Accounting for spectroscopic effects in laser-based open-path eddy covariance flux measurements. Glob. Chang. Biol. 25, 2189–2202. https://doi.org/10.1111/gcb.14614.

Burgon, R., Sargent, S., Conrad, B., 2016. Performance evaluation of an innovative sampling system for closed path eddy covariance measurements. In: AMS 32nd Conference on Agric. For. Meteorol. Poster, 140.

Cole, J.J., Caraco, N.F., 1998. Atmospheric exchange of carbon dioxide in a low-wind oligotrophic lake measured by the addition of SF6. Limnol. Oceanogr. 43 (4), 647–656.

Cui, Y., Zhu, L., Wang, H., Zhao, Z., Ma, S., Ye, Z., 2023. Characteristics and oxidative potential of ambient PM2.5 in the yangtze river delta region: pollution level and source apportionment. Atmosphere 14, 425. https://doi.org/10.3390/atmos14030425.

Deventer, M.J., Roman, T., Bogoev, I., Kolka, R.K., Erickson, M., Lee, X., Baker, J.M., Millet, D.B., Griffis, T.J., 2021. Biases in open-path carbon dioxide flux measurements: roles of instrument surface heat exchange and analyzer temperature sensitivity. Agric. For. Meteorol. 296, 108216 https://doi.org/10.1016/j.agrformet.2020.108216.

Duan, Z., Gao, H., Gao, Z., Wang, R., Xue, Y., Yao, X., 2013. An approach to minimizing artifacts caused by cross-sensitivity in the determination of air–sea flux using the eddy-covariance technique. Boundary-Layer Meteorol 148, 227–239. https://doi.org/10.1007/s10546-013-9814-1.

Foken, T., Leuning, R., Oncley, S.R., Mauder, M., Aubinet, M., 2012. Corrections and data quality control. Eddy Covariance 85–131. https://doi.org/10.1007/978-94-007-2351-1_4.

Frank, J.M., Massman, W.J., 2020. A new perspective on the open-path infrared gas analyzer self-heating correction. Agric. For. Meteorol. 290, 107986 https://doi.org/10.1016/j.agrformet.2020.107986.

Grelle, A., Burba, G., 2007. Fine-wire thermometer to correct CO_2 fluxes by open-path analyzers for artificial density fluctuations. Agric. For. Meteorol. 147, 48–57. https://doi.org/10.1016/j.agrformet.2007.06.007.

Griffiths, H., 1992. Carbon isotope discrimination and the integration of carbon assimilation pathways in terrestrial CAM plants. Plant Cell Environ 15, 1051–1062. https://doi.org/10.1111/j.1365-3040.1992.tb01655.x.

Ham, J.M., Heilman, J.L., 2003. Experimental test of density and energy-balance corrections on carbon dioxide flux as measured using open-path eddy covariance. Agron. J. 95, 1393–1403. https://doi.org/10.2134/agronj2003.1393.

Haslwanter, A., Hammerle, A., Wohlfahrt, G., 2009. Open-path vs. closed-path eddy covariance measurements of the net ecosystem carbon dioxide and water vapour exchange: a long-term perspective. Agric. For. Meteorol. 149, 291–302. https://doi.org/10.1016/j.agrformet.2008.08.011.

Helbig, M., Wischnewski, K., Gosselin, G.H., Biraud, S.C., Bogoev, I., Chan, W.S., Euskirchen, E.S., Glenn, A.J., Marsh, P.M., Quinton, W.L., Sonnentag, O., 2016. Addressing a systematic bias in carbon dioxide flux measurements with the EC150 and the IRGASON open-path gas analyzers. Agric. For. Meteorol. 228, 349–359. https://doi.org/10.1016/j.agrformet.2016.07.018.

Heusinkveld, B.G., Jacobs, A.F., Holtslag, A.A., 2008. Effect of open-path gas analyzer wetness on eddy covariance flux measurements: a proposed solution. Agric. For. Meteorol. 148, 1563–1573. https://doi.org/10.1016/j.agrformet.2008.05.010.

Holaday, A.S., Bowes, G., 1980. C_4 acid metabolism and dark CO_2 fixation in a submersed aquatic macrophyte (Hydrilla verticillata). Plant Physiol 65, 331–335. https://doi.org/10.1104/pp.65.2.331.

Horst, T.W., Lenschow, D.H., 2009. Attenuation of scalar fluxes measured with spatially-displaced sensors. Boundary-Layer Meteorol 130, 275–300. https://doi.org/10.1007/s10546-008-9348-0.

Huang, Y., Song, J., Wang, J., Fan, C., 2012. Air-sea carbon-dioxide flux estimated by eddy covariance method from a buoy observation. Acta Oceanol. Sin. 31, 66–71. https://doi.org/10.1007/s13131-012-0253-5.

Kondo, F., Ono, K., Mano, M., Miyata, A., Tsukamoto, O., 2014. Experimental evaluation of water vapour cross-sensitivity for accurate eddy covariance measurement of CO_2 flux using open-path CO_2/H_2O gas analysers. Tellus B Chem. Phys. Meteorol. 66, 23803. https://doi.org/10.3402/tellusb.v66.23803.

Kohsiek, W., 2000. Water vapor cross-sensitivity of open path H_2O/CO_2 sensors. J. Atmos. Oceanic Technol. 17 (3), 299–311, 2000.

Landwehr, S., Miller, S.D., Smith, M.J., Saltzman, E.S., Ward, B., 2014. Analysis of the PKT correction for direct CO_2 flux measurements over the ocean. Atmos. Chem. Phys. 14, 3361–3372. https://doi.org/10.5194/acp-14-3361-2014.

Lee, X., Liu, S., Xiao, W., Wang, W., Gao, Z., Cao, C., Hu, C., Hu, Z., Shen, S., Wang, Y., Wen, X., Xiao, Q., Xu, J., Yang, J., Zhang, M., 2014. The Taihu eddy flux network: an observational program on energy, water, and greenhouse gas fluxes of a large

freshwater lake. Bull. Amer. Meteor. Soc. 95, 1583–1594. https://doi.org/10.1175/BAMS-D-13-00136.1.

Leuning, R., Denmead, O.T., Lang, A.R.G., Ohtaki, E., 1982. Effects of heat and water vapor transport on eddy covariance measurement of CO_2 fluxes. Boundary-Layer Meteorol 23, 209–222. https://doi.org/10.1007/BF00123298.

Ma, J., Zha, T., Jia, X., Sargent, S., Burgon, R., Bourque, C.P.A., Zhou, X., Liu, P., Bai, Y., Wu, Y., 2017. An eddy-covariance system with an innovative vortex intake for measuring carbon dioxide and water fluxes of ecosystems. Atmos. Meas. Tech. 10, 1259–1267. https://doi.org/10.5194/amt-10-1259-2017.

McGillis, W.R., Edson, J.B., Hare, J.E., Fairall, C.W., 2001. Direct covariance air-sea CO_2 fluxes. J. Geophys. Res. Oceans 106, 16729–16745. https://doi.org/10.1029/2000JC000506.

Mook, W.G., Bommerson, J.C., Staverman, W.H., 1974. Carbon isotope fractionation between dissolved bicarbonate and gaseous carbon dioxide. Earth Planet. Sci. Lett. 22, 169–176. https://doi.org/10.1016/0012-821X(74)90078-8.

Nilsson, E., Bergström, H., Rutgersson, A., Podgrajsek, E., Wallin, M.B., Bergström, G., Dellwik, E., Landwehr, S., Ward, B., 2018. Evaluating humidity and sea salt disturbances on CO_2 flux measurements. J. Atmos. Oceanic Technol. 35, 859–875. https://doi.org/10.1175/JTECH-D-17-0072.1.

Ono, K., Miyata, A., Yamada, T., 2008. Apparent downward CO_2 flux observed with open-path eddy covariance over a non-vegetated surface. Theor. Appl. Climatol. 92, 195–208. https://doi.org/10.1007/s00704-007-0323-3.

Owen, N.A., Choncubhair, Ó.N., Males, J., del Real Laborde, J.I., Rubio-Cortés, R., Griffiths, H., Lanigan, G., 2016. Eddy covariance captures four-phase crassulacean acid metabolism (CAM) gas exchange signature in Agave. Plant Cell Environ 39, 295–309. https://doi.org/10.1111/pce.12610.

Pan, D., Gelfand, I., Tao, L., Abraha, M., Sun, K., Guo, X., Chen, J., Robertson, G.P., Zondlo, M.A., 2022. A new open-path eddy covariance method for nitrous oxide and other trace gases that minimizes temperature corrections. Glob. Chang. Biol. 28, 1446–1457. https://doi.org/10.1111/gcb.15986.

Prytherch, J., Yelland, M.J., Pascal, R.W., Moat, B.I., Skjelvan, I., Neill, C.C., 2010. Direct measurements of the CO_2 flux over the ocean: development of a novel method. Geophys. Res. Lett. 37 https://doi.org/10.1029/2009GL041482.

Runkle, B.R., Wille, C., Gažovič, M., Kutzbach, L., 2012. Attenuation correction procedures for water vapour fluxes from closed-path eddy-covariance systems. Boundary-Layer Meteorol 142, 401–423. https://doi.org/10.1007/s10546-011-9689-y.

Wang, W., Xiao, W., Cao, C., Gao, Z., Hu, Z., Liu, S., Shen, S., Wang, L., Xiao, Q., Xu, J., Yang, D., Lee, X., 2014. Temporal and spatial variations in radiation and energy balance across a large freshwater lake in China. J. Hydrol. 511, 811–824. https://doi.org/10.1016/j.jhydrol.2014.02.012.

Wang, W., Xu, J., Gao, Y., Bogoev, I., Cui, J., Deng, L., Hu, C., Liu, C., Liu, S., Shen, J., Sun, X., Xiao, W., Yuan, G., Lee, X., 2016. Performance evaluation of an integrated open-path eddy covariance system in a cold desert environment. J. Atmos. Oceanic Technol. 33, 2385–2399. https://doi.org/10.1175/JTECH-D-15-0149.1.

Wang, L., Lee, X., Wang, W., Wang, X., Wei, Z., Fu, C., Gao, Y., Lu, L., Song, W., Su, P., Lin, G., 2017. A meta-analysis of open-path eddy covariance observations of apparent CO_2 flux in cold conditions in FLUXNET. J. Atmos. Oceanic Technol. 34, 2475–2487. https://doi.org/10.1175/JTECH-D-17-0085.1.

Watanabe, K., Kuwae, T., 2015. Radiocarbon isotopic evidence for assimilation of atmospheric CO_2 by the seagrass Zostera marina. Biogeosciences 12, 6251–6258. https://doi.org/10.5194/bg-12-6251-2015.

Webb, E.K., Pearman, G.I., Leuning, R., 1980. Correction of flux measurements for density effects due to heat and water vapour transfer. Q. J. R. Meteorol. Soc. 106, 85–100. https://doi.org/10.1002/qj.49710644707.

Winter, K., Holtum, J.A., 2002. How closely do the $\delta^{13}C$ values of crassulacean acid metabolism plants reflect the proportion of CO_2 fixed during day and night? Plant Physiol 129, 1843–1851. https://doi.org/10.1104/pp.002915.

Xie, Y., Zhang, M., Xiao, W., Zhao, J., Huang, W., Zhang, Z., Hu, Y., Qin, Z., Jia, L., Pu, Y., Chu, H., Wang, J., Shi, J., Liu, S., Lee, X., 2022. Nitrous oxide flux observed with tall-tower eddy covariance over a heterogeneous rice cultivation landscape. Sci. Total Environ. 810, 152210 https://doi.org/10.1016/j.scitotenv.2021.152210.

Yin, L., Li, W., Madsen, T.V., Maberly, S.C., Bowes, G., 2017. Photosynthetic inorganic carbon acquisition in 30 freshwater macrophytes. Aquat. Bot. 140, 48–54. https://doi.org/10.1016/j.aquabot.2016.05.002.

Zhang, M., Xiao, Q.T., Zhang, Z., Gao, Y.Q., Zhao, J.Y., Pu, Y.N., Wang, W., Xiao, W., Liu, S.D., Lee, X., 2019. Methane flux dynamics in a submerged aquatic vegetation zone in a subtropical lake. Sci. Total Environ. 672, 400–409. https://doi.org/10.1016/j.scitotenv.2019.03.466.

Zhang, Z., Zhang, M., Cao, C., Wang, W., Xiao, W., Xie, C., Chu, H., Wang, J., Zhao, J., Jia, L., Liu, Q., Huang, W., Zhang, W., Lu, Y., Xie, Y., Wang, Y., Pu, Y., Hu, Y., Chen, Z., Qin, Z., Lee, X., 2020. A dataset of microclimate and radiation and energy fluxes from the Lake Taihu eddy flux network. Earth Syst. Sci. Data 12, 2635–2645. https://doi.org/10.5194/essd-12-2635-2020.